[Article ID] 1003- 6326(2002)04- 0669- 07

Anisotropic plastic deformation behavior of B2-ordered Fe_3Al single crystals at room temperature①

ZHENG Wei-wei(郑为为)[1], YANG Wang-yue(杨王玥)[2], SUN Zu-qing(孙祖庆)[1]
(1. State Key Laboratory for advanced Metals and Materials,
University of Science & Technology Beijing, Beijing 100083, China;
2. School of Materials Science and Engineering,
University of Science & Technology Beijing, Beijing 100083, China)

[Abstract] The tensile plastic deformation behavior of B2-ordered Fe_3Al single crystals at room temperature was systematically investigated. The results show that the mechanical properties are strongly orientation dependent. The plastic elongation of crystals with orientation near [110] is as high as 42%. Slip trace analysis shows that although slip planes are found to change among {110}, {112} and {123} with the change in orientations, the initial slip planes in all cases are {110}. Five-stage work hardening curve including four linear stages and one parabolic stage is obtained; but not all stages are observed in the actual deformation of each crystal. In combination with investigations of dislocation substructure, it is found that deformations in stage Ⅰ ~ Ⅲ are corresponding to the motion of two-fold superdislocations. The higher work hardening rate of stage Ⅱ is mainly due to the stronger interactions between primary dislocations and secondary dislocations than those in stage Ⅲ. Deformation in stage Ⅳ involved is not only the motion of two-fold superdislocations but also the slip of dissociated superpartials with APB traps and the formation of APB tube, both of which are attributed to the hardening. Deformation in stage Ⅴ is controlled by the cross slip of dissociated superpartials. The dominated softening effect of cross slip reduces the hardening rate and leads to the formation of parabolic stage.

[Key words] plastic deformation; B2-order; Fe_3Al; single crystal
[CLC number] TG 113.25; TG 133 [Document code] A

1 INTRODUCTION

Iron aluminides based on Fe_3Al have relatively low density, high specific strength, low cost, good oxidation resistance and excellent sulphidation resistance at high temperature in comparison with stainless steels. Based on these benefits iron aluminides have potential applications instead of stainless steels in many different fields. Moreover, its room temperature ductility has been dramatically improved through adding chromium[1,2] and controlling hot work processing[3,4]. It has been widely accepted that the best room temperature tensile strength and ductility can be obtained in specimen which is warm rolled at 550~650 ℃ and annealed at just below the recrystallization starting temperature followed by oil quenching. The mechanism of improved properties is contributed to at least four aspects including the grain boundary[4], specific dislocation configurations[5], B2 phase structure[6,7] and texture[8]. But its deformation behavior as well as the effect of orientation is not well understood.

Fe_3Al-based alloy can be of long-range ordered DO_3 structure or imperfectly ordered B2 structure at room temperature depending on the heat treatment used. Major works of plastic deformation behavior were focused on DO_3-ordered alloys[9~11] and few is about B2-ordered alloys. Our recent work has indicated that B2-ordered Fe_3Al single crystals show significantly anisotropic mechanical property when they are deformed in tension at room temperature in vacuum[12~14]. In the present paper, the authors summarize the characteristics of the mechanical properties, shear stress—strain curves, slip systems and dislocation configurations of B2-ordered Fe_3Al single crystal.

2 EXPERIMENTAL

Fe_3Al alloy ingots containing 30% aluminum (mole fraction) were fabricated by vacuum induction melting of high purity elements. Large single crystal slabs, about 150 mm × 45 mm × 15 mm in size, were grown by the Bridgman technique. The crystals were annealed for 48 h at 1050 ℃. Tensile sheet specimens with gage size of 10 mm × 3 mm × 1.5 mm were electro-discharge machining (EDM) wire cut from the slabs for each of the desired crystllographic orientation. Specimens were heat treated at 700 ℃ for 2 h and then oil quenched. By this method, the crystals were considered to have a higher degree of B2 ordering[10]. They were electropolished in a solution of sulphuric acid and methanol (the volume ratio is 1:

① [Foundation item] Project (59681005) supported by National Natural Science Foundation of China
[Received date] 2001- 10- 08

13) at 293 K. The tensile axes were determined by electron back scattered diffraction (EBSD) technique. Single crystal specimens were strained in tension in Gleeble 1 500 thermal simulation machine at room temperature in vacuum with a strain rate of $3 \times 10^{-3} s^{-1}$. Tensile tests were conducted in vacuum in order to remove the effect of hydro-embrittlement[1,4]. At least, two specimens were tested for each orientation.

The slip traces of different strained specimens were observed with an optical microscope. The slip planes were determined from the slip traces on two surfaces of each crystal. Because the slip direction of Fe_3Al alloys has already been testified as $\langle 111 \rangle$[15], the Schmid factor of the initial slip systems were acquired. The shear stress (τ)—shear strain (γ) curves were converted from the automatically recorded load—elongation data by using the equations given by Schmid and Boas[16].

For TEM observation, thin foils were all cut parallel to the sheet surface from the gage of deformed specimens, and subsequently thinned and electropolished in a 20% nitric acid-methanol solution at a voltage of 8 V and 243 K. The associated dislocation substructures were studied on a Hitachi H-800 transmission electron microscope at the accelerating voltage of 200 kV.

3 RESULTS AND DISCUSSION

3.1 Mechanical properties

The tensile mechanical properties of B2-ordered Fe_3Al single crystals are given in Table 1[12]. It can be seen that good ductility is achieved at ambient temperature for the B2-ordered as-cast Fe_3Al single crystal and the plastic elongation are strongly orientation dependent. [681]-oriented 2# single crystal has 42% plastic elongation. [449]-oriented 4# crystal achieves 29% plastic elongation. In contrast, near [001] orientation, the plastic elongation was only 8%. Such a good tensile ductility at room temperature has not been reported at B2-ordered as-cast NiAl[17] and FeAl[18] intermetallics.

From Table 1, it can also be seen that the yield strength varies between 306 MPa and 566 MPa with change in tensile orientation. In general, the yield strength for crystals with orientations near [111] is high, and that for orientations near [110] is low. Particularly the yield strength of [565]-oriented single crystal reaches up to 566 MPa. This strength value can be compared with that of B2 thermomechanical treated Fe-28Al-5Cr-0.1Zr-0.5Mo-0.5Nb-0.05B polycrystal[4].

It is well known that the yield strength is determined not only by the Schmid factor of initial slip systems but also by the critical resolved shear stress (CRSS). In case of similar CRSS, the bigger the Schmid factor is, the lower the yield strength is. According to our studies, the CRSS value of B2-ordered Fe_3Al single crystal is not constant but orientation dependent, as shown in Table 2, which is similar to some non-ordered BCC metals. For orientations having similar CRSS value, orientations near [111] have smaller Schmid factors leading to a higher yield strength.

Table 1 Room temperature tensile properties of B2-ordered Fe_3Al single crystals[12]

Crystal No.	Tensile axis	Yield strength, σ_s/MPa	Plastic elongation, δ/%	Fracture strength /MPa
1	[001]	380	11.1	495
2	[681]	308	42	681
3	[665]	442	9.8	497
4	[449]	365	29	541
5	[106]	345	10.6	480
6	[107]	343	8.4	437
7	[329]	327	14.8	454
8	[438]	306	20.8	451
9	[557]	354	13.6	424
10	[675]	403	9.4	456
11	[538]	345	20.8	465
12	[419]	353	14.8	462
13	[121]	401	8	471
14	[528]	332	23	474
15	[565]	566	10.8	690
16	[637]	471	13.6	570
17	[575]	414	8.4	457
18	[745]	329	15.6	431

3.2 Slip systems and slip line patterns

By observing slip traces of yielding specimens with various orientations, the initial slip systems were determined. Combining with the yield strength, the CRSS values of each orientation were calculated and tabulated in Table 2. It is easy to find that all the initial slip planes are of {110} type. But the CRSS values of {110}$\langle 111 \rangle$ are not the same. Those of crystals with orientations in the middle part of the standard 001-111-101 orientation triangle are relatively higher. Although the reason for this discrepancy is not certain, it may be related to the moving of two-fold superdislocations, antiphase boundary (APB) energies and the jog formation on screw dislocations[19].

It should also be noted that except for crystals with orientations near [001] (including crystal 1#, 5#, 6# and 7#), where double slip was found to occur, all the other crystals were found to slip on one system at beginning of deformation. In the early stage of deformation (for tensile engineering strain of about 1%), slip lines corresponding to single slip plane tend to cluster in several bands at some local areas and then spread throughout the gauge, as shown in Fig. 1(a). With further deformation (for tensile

Table 2 Elementary slip systems and $CRSS_{\{110\}\langle 111\rangle}$ B2-ordered Fe_3Al single crystals deformed at room temperature in tension

Group No.	Crystal No.	Orientation	Initial slip systems	Schmid factors of initial slip systems	CRSS/MPa
A: Near [001]	1	[001]	$(011)[1\bar{1}1]$ $(0\bar{1}1)[111]$	0.436 0.439	153
	6	[107]	$(011)[1\bar{1}1]$ $(0\bar{1}1)[111]$	0.461 0.457	157
	5	[106]	$(011)[1\bar{1}1]$ $(0\bar{1}1)[111]$	0.467 0.466	161
	7	[329]	$(011)[1\bar{1}1]$ $(110)[1\bar{1}1]$	0.47 0.191	156
B: Near [110]	2	[681]	$(011)[\bar{1}\bar{1}1]$	0.465	143
C: In middle part of triangle	11	[538]	$(011)[1\bar{1}1]$	0.462	159
	12	[419]	$(011)[1\bar{1}1]$	0.499	176
	14	[528]	$(011)[1\bar{1}1]$	0.483	160
	16	[637]	$(011)[1\bar{1}1]$	0.437	206
D: Near [112]	4	[449]	$(011)[1\bar{1}1]$	0.431	157
	8	[438]	$(011)[1\bar{1}1]$	0.447	137
	13	[121]	$(110)[\bar{1}11]$	0.426	171
	9	[557]	$(011)[1\bar{1}1]$	0.348	123
	18	[745]	$(110)[1\bar{1}1]$	0.385	127
E: Near [111]	17	[575]	$(110)[1\bar{1}1]$	0.363	150
	3	[665]	$(011)[\bar{1}\bar{1}1]$	0.33	150
	10	[675]	$(011)[\bar{1}\bar{1}1]$	0.372	146
	15	[565]	$(011)[\bar{1}\bar{1}1]$	0.322	182

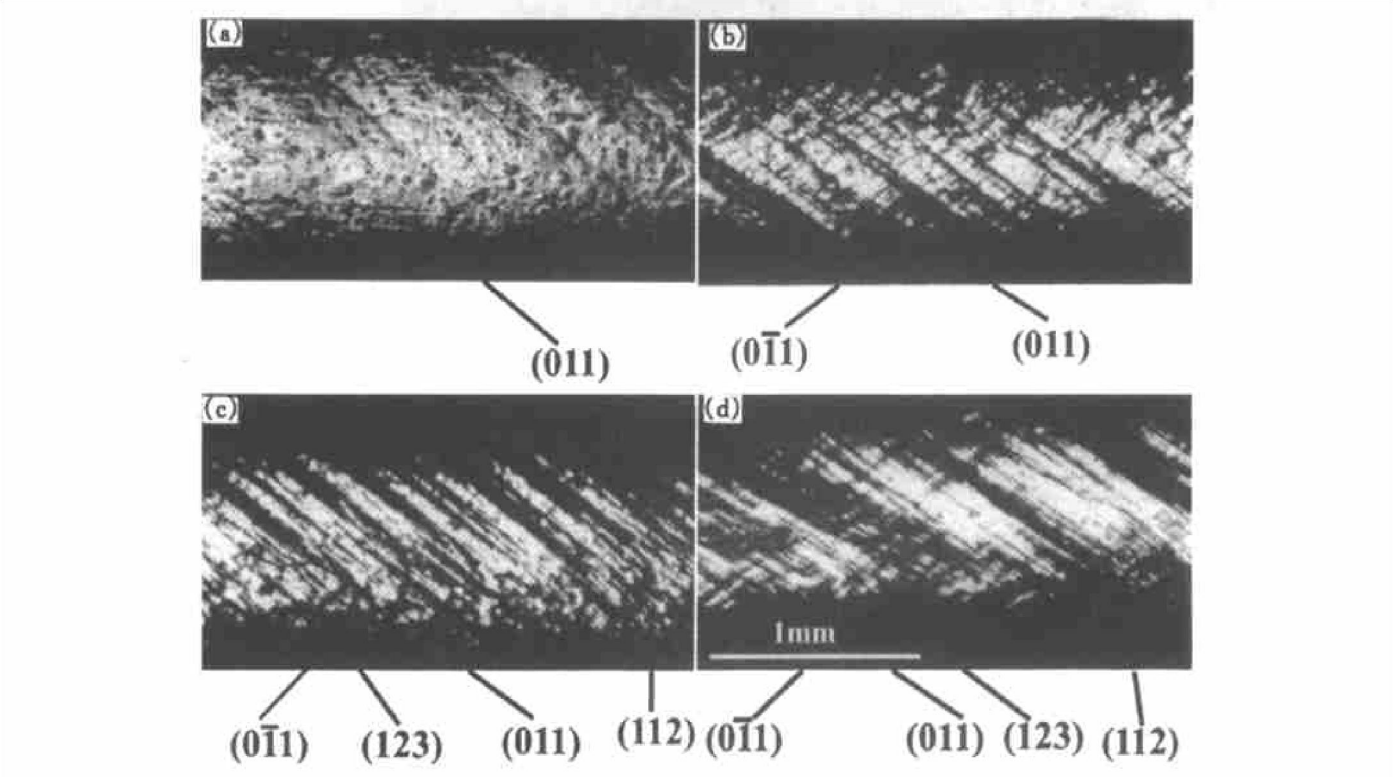

Fig. 1 Slip traces on near (001) side face of [681]-oriented 2# crystal with different engineering strains
(a) —1%; (b) —7%; (c) —12%; (d) —16%

engineering strain of about 7%), slip lines of another direction which are corresponding to secondary slip system appears, as illustrated in Fig. 1(b). But the number of these lines is less than that of the primary system. As deformation goes on, traces corresponding to secondary systems become faint, as shown in Fig. 1(c). This indicates that the effect of secondary slip systems becomes weaker, that is, the initial primary system is dominated in this stage of deformation.

With increasing strain (for tensile engineering strain of about 16%), the primary slip bands begin to form, as shown in Fig. 1(d). Within these bands traces of secondary systems gradually become stronger, and some of them are deep and coarse which can be comparable with that of primary systems. In later stage of deformation, slip traces of both primary systems and secondary systems are wavy as illustrated in Fig. 2. Traces in primary slip bands are corresponding to several planes of {110}, {112} and {123} type with the same slip direction. Similarly wavy traces of secondary slip systems are corresponding to several planes with the same [111] slip direction. Early studies have confirmed that wavy slip traces are formed by the cross slip of screw superdislocations[20], which is attributed to the formation of parabolic shear stress—strain curve.

3.3 Shear stress—shear strain curves

Fig. 3 shows the shear stress—strain curves of eighteen B2-ordered Fe_3Al single crystals[14]. As we can see, all the stress—strain curves show yield points. But the shape of curves and the work hardening rate are strongly orientation dependent. For crystals with tensile axes near [001] (such as crystal 1#, 5#, 6# and 7#), the initial work hardening rate

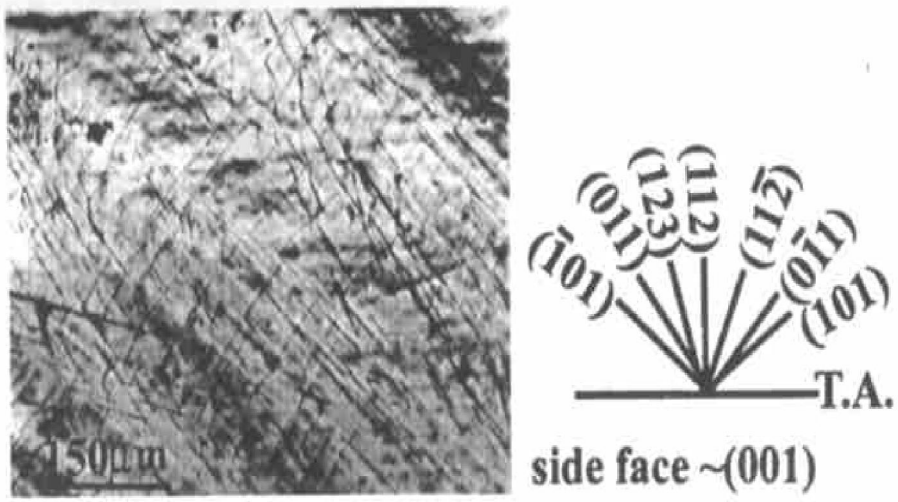

Fig. 2 Wavy slip lines of [681]-oriented 2# crystal with strain of 42%

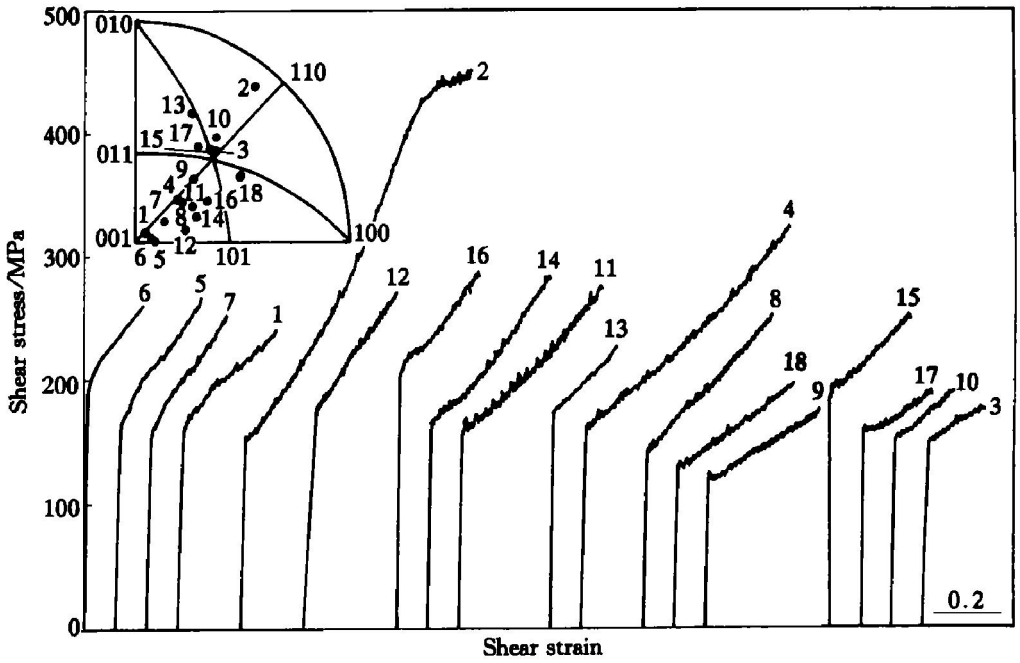

Fig. 3 Shear stress-shear strain curves of B2-ordered Fe_3Al single crystals deformed in tension at room temperature in vacuum

after yield point is in general higher than those of other crystals. Slip trace analysis has revealed that double slip occurs in these four crystals at the early stage of deformation. While for other crystals, slip invariably starts on one system. This indicates that the initial work hardening rate of shear stress—strain curve depends on the number of activated slip systems.

Fig. 4 clearly shows the shear stress—strain curve of near [001]-oriented crystal 1#. The curve can be divided into two stages with different work hardening rate. As mentioned above the first higher hardening rate stage is corresponding to double slip. Being distinguished from single slip easy glide stage, this double slip stage is called stage II. Actually, only crystals around [001] have stage II. The work hardening rate of the second linear stage is lower than that of the first one.

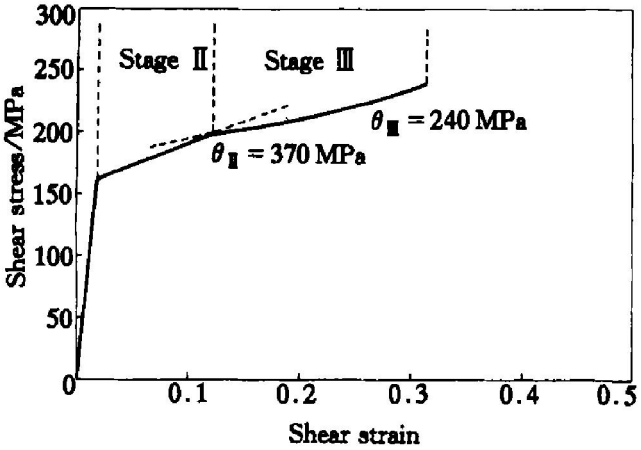

Fig. 4 Shear stress—strain curve of [001]-oriented 1# crystal

Fig. 5 shows the shear stress—strain curve of [681]-oriented single crystal. This curve includes three linear stages and one parabolic stage. The initial very short stage is formed by single slip on (011) plane. The following two linear stages, which are called stage III and stage IV respectively, are corresponding to multiple slip with one dominating system and this is confirmed by slip line observations. The parabolic stage V is thought to be the result of the cross slip of screw dislocations, which is consistent with the wavy slip traces (as shown in Fig. 2). The definition of stage I to V are described in more detail in other papers[14]. From Fig. 3, we can clearly see that quick hardening stage IV and parabolic stage V are observed only in [681]-oriented crystal and the work hardening rate of stage III is different with the change in orientation.

3.4 Dislocation configurations

The change in dislocation configurations as a function of strain at room temperature for [681]-oriented crystal is shown in Fig. 6. Long screw superdislocations with the end of edge segments are the main feature of crystal with strain of 1% (as shown in Fig. 6(a)). No cusps and jogs are observed on screw

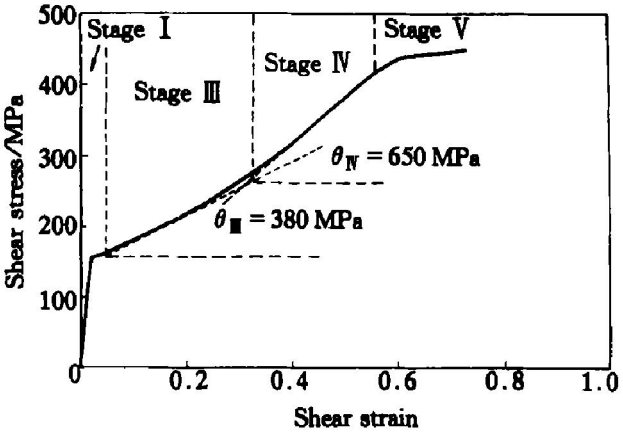

Fig. 5 Shear stress—strain curve of [681]-oriented 2# crystal

segments indicating the very weak interactions between dislocation. Correspondingly the work hardening rate is relatively low.

After 7% tensile strain, the dislocations are predominantly $[\bar{1}\bar{1}1]$ type screws (as shown in Fig. 6(b)). The long screw superdislocations are heavily jogged. Narrow edge trails and dipoles are seen behind the cusps on screws, which are thought to be formed by the motion of pinned screw segments. This structure is in fact very similar to that found in non-ordered BCC Fe-3% Si alloys[21]. Large number of dipoles, edge trails and heavily jogged screws indicate the strong interactions between dislocations. The increase of dislocation density implies the abundant multiplication of dislocations. At some local areas, another [111] type screw superdislocations are observed to interact with the primary type dislocations. The hardening in this stage is partially due to the interactions between primary dislocations and [111] secondary dislocations, and partially due to the motion of jogged screw dislocations.

In the specimen with strain of 16% (as shown in Fig. 6(c)), the densities of the primary and secondary [111] screw superdislocations are almost the same and both increased considerably comparing with that in Fig. 6(b). They crisscross each other but no evidence shows they are reacting to produce ⟨001⟩ dislocations. In this case type screw superdislocations are also observed and some have begun to dissociate as shown in Fig. 6(c) marked 1 and 2. The highly dense screw dislocations indicating abundant multiplication and the strong interaction between primary and secondary dislocations lead to high work hardening rate. From Fig. 6(c), we also noted that the number of edge dipoles seem to decrease. This may be due to the dipole breaking at such a high applied stress[22].

By using 002 superlattice diffraction, straight B2-type APB (NNAPB) traps were observed as shown in Fig. 7. Early studies have suggested that once the applied stress is sufficiently high, the twofold $a/2\langle 111\rangle$ superdislocations can be split into two

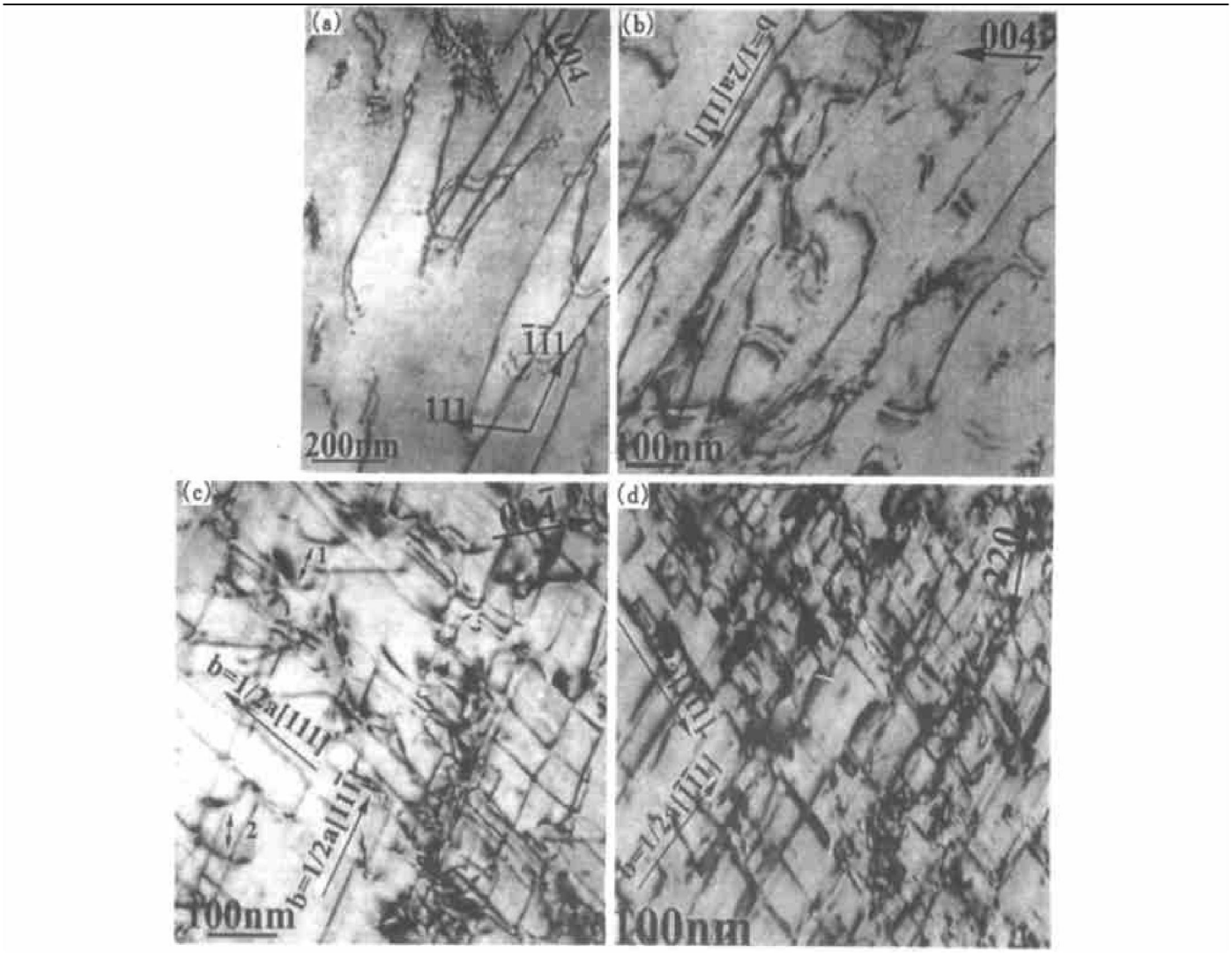

Fig. 6 Dislocation configurations in [681]-oriented crystal with different strains
(a) —1%, $\boldsymbol{B}$= [$\bar{1}$01]; (b) —7%, $\boldsymbol{B}$= [$\bar{1}$10]; (c) —16%, $\boldsymbol{B}$= [1$\bar{1}$0]; (d) —42%, $\boldsymbol{B}$= [1$\bar{1}$0]

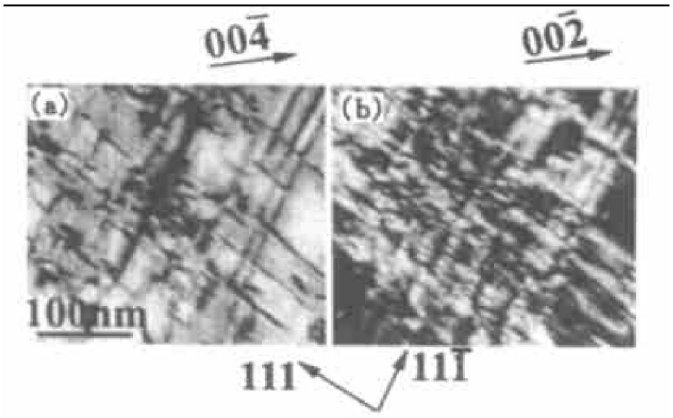

Fig. 7 Bright field image and dark field image showing APB tubes along [111] direction with 00$\bar{4}$ and 00$\bar{2}$ reflection in [681]-oriented 2# single crystal strained to 16%

a/4〈111〉 superpartials (where a is the lattice constant of Fe_3Al). According to the study of Crawford and Ray[23], the APB energy of B2-ordered Fe-30% Al alloy is about 60 mJ/m^2. The dissociation of two-fold dislocations must overcome the APB energy. Therefore, the stress for the a/2〈111〉 superdislocation to dissociate is at least 239 MPa. From the shear stress—strain curve shown in Fig. 5, we know that the corresponded stress at this strain exceeds 260 MPa, which is high enough to dissociated the two-fold superdislocations. The moving of dissociated superpartials will produce APB traps leading to the increase of work hardening rate. In addition, at local area, the narrow NNAPB streaks along [$\bar{1}\bar{1}$1] and [111] directions are considered as APB tubes which are thought to be the result of the conservative motion of jogs on screw superdislocations. Similar APB tubes have been observed in B2-ordered Fe-35.5% Al (mole fraction) by Crawford and are proved to be contributed to the work hardening of ordered alloys[24]. Therefore the much higher work hardening rate of stage Ⅳ comparing with that of stage Ⅲ is mainly due to the APB tube and APB trap formations.

At higher strain (42% and fractured), the density of primary and secondary dislocations and small dislocation loops and debris further increases. Under $\boldsymbol{g}$~ 3$\boldsymbol{g}$ weak beam condition all the primary and secondary screw superdislocations are of single-line[13]. This was also confirmed by the abundant NNAPB faults, as shown in Fig. 8. The curved NNAPB traps imply the existence of cross slip, which is consistent

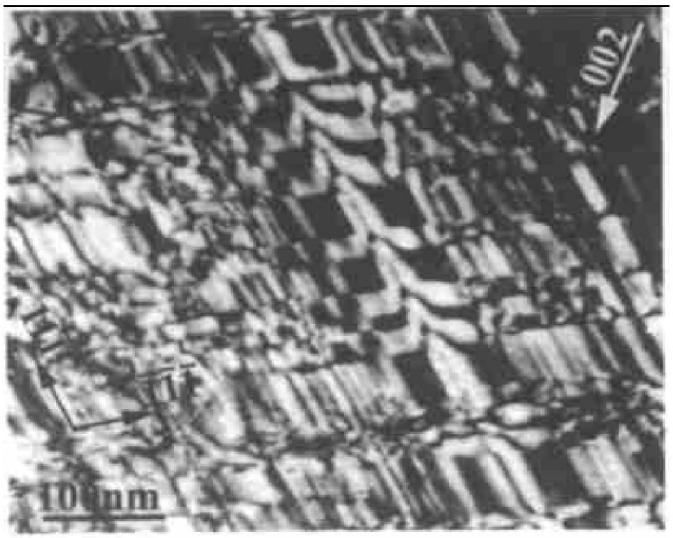

Fig. 8 Dark field image taken using a $00\bar{2}$ beam showing NNAPB trails in [681]-oriented 2# single crystal fractured at room temperature($\boldsymbol{B}$= [$1\bar{1}0$])

with the wavy slip trace (as shown in Fig. 2). The single-lined screw dislocations are easy to cross slip comparing with the two-fold superdislocations, leading to softening and the formation of parabolic stage on shear stress—strain curve.

ACKNOWLEDGEMENT

The authors would like to acknowledge Dr. Liu Qing in the orientation measurement.

[REFERENCES]

[1] Mckamey C G, Horton J A, Liu C T. Effect of chromium on properties of Fe_3Al [J]. J Mater Res 1989, 4: 1156– 1163.

[2] SUN Zu-qing, HUANG Yuan-ding, YANG Wang-yue, et al. The ductility of Fe_3Al intermetallic compounds (Ⅰ) [J]. J of University of Science and Technology Beijing, 1991, 13(6): 539– 543.

[3] SUN Zu-qing, HUANG Yuan-ding, YANG Wang-yue, et al. The method for optimizing the room temperature mechanical properties of Fe_3Al-based aluminides [J]. Acta Metall Sinica, 1993, 29(8): A354– A358.

[4] SUN Zu-qing, HUANG Yuan-ding, YANG Wang-yue, et al. Microstructure engineering for optimizing the room temperature mechanical properties of Fe_3Al-based aluminides [J]. Mat Res Soc Symp Proc, 1993, 288: 885 – 890.

[5] Morris D G, Leboeuf M. The role of controlled recrystallization treatments on ductility of Fe_3Al alloys [J]. Acta Metall Mater, 1994, 42: 1817– 1823.

[6] Wright R N. The influence on thermomechanical processing on microstructure and mechanical properties of Fe_3Al alloys [A]. Proceedings of the Fourth Annual Conference on Fossil Energy Materials, ORNL/FMP-90/1 [C]. U. S. Department of Energy, Oak Ridge, TN 1990. 231.

[7] Maziasz P J, Mchamey C G, Cavin O B, et al. Some effects of composition and microstructure on the B2-DO_3 ordered phase transition in Fe_3Al alloys [J]. Mat Res Soc Symp Proc, 1993, 288: 209– 215.

[8] SUN Zu-qing, MAO Wei-min, CHAI Shu-yan, et al. Texture and mechanical properties of warm rolled Fe_3Al based alloy [J]. Acta Metall sinica, 1995, 8: 369– 374.

[9] Leamy H J, Kayser F X, Marcinkowski M J. The plastic deformation behaviour of long-range ordered Iron-Aluminium alloys Ⅰ [J]. Single crystal deformation experiment Phil Mag, 1969, 20: 763– 777.

[10] Marcinkowski M J, brown N. Theory and direct observation of dislocations in the Fe_3Al superlattices [J]. Acta Metall, 1961, 9: 764– 786.

[11] Leamy H J, Kayser F X. The compressive deformation behavior of long range ordered polycrystalline Iron-Aluminum alloys [J]. Phys Stat Sol, 1969, 34: 765– 780.

[12] ZHENG Wei-wei, YANG Wang-yue, SUN Zu-qing, et al. Room temperature mechanical behavior of B2-ordered Fe_3Al single crystals [J]. Acta Metall Sinica, (in Chinese), 1998, 34: 1137– 1142.

[13] ZHENG Wei-wei, YANG Wang-yue, SUN Zu-qing, Room temperature mechanical behavior of B2-ordered Fe_3Al single crystals [J]. Mat Sci Eng, 2001, A299, 46– 50.

[14] ZHENG Wei-wei, YANG Wang-yue and SUN Zu-qing. Orientation dependency of shear stress-strain curves in B2-ordered Fe_3Al single crystals deformed in tension at room temperature [J]. Sci in China, 2002, 45(3): 314– 320.

[15] Mckamey C G, Devan J H, Tortoreili P F, et al. A review of recent developments in Fe_3Al-based alloys [J]. J Mater Res, 1991, 6: 1779– 1805.

[16] Schmid E, Boas W. Plasticity of Crystals [M]. London: F. A. Hug & Company Ltd, 1950. 95.

[17] Lahrman D F, Field R D, Darolia. The effect of crystallographic orientation on the mechanical properties of a single crystal NiAl+ Fe alloy [A]. Mat Res Soc Symp Proc [C]. 1993. 288: 679– 684.

[18] Gavdosh D J, Draper S L Noebe R D, et al. Room temperature flow and fracture of Fe-49% Al alloys [J]. Mat Sci Eng, 1992, A 150: 7– 20.

[19] Takeuchi S, Furubayashi E, Taoka T. Orientation dependence of yield stress in 4.4% silicon iron single crystals [J]. Acta Metall, 1967, 15: 1179– 1191.

[20] Stoloff N S, Davies R G. The plastic deformation of ordered FeCo and Fe_3Al alloys [J]. Acta Metall, 1964, 12: 473– 485.

[21] Low J R Jr, Turkalo A M. Slip band structure and dislocation multiplication in silicon iron crystals [J]. Acta Metall, 1962, 10: 215– 227.

[22] Sadananda K, Marcinkowski M J. Work hardening in ordered and disordered alloys [J]. J Appl Phys, 1973, 44: 1989– 1996.

[23] Crawford R C, Ray I L F. Antiphase boundary energies in iron-aluminium alloys [J]. Phil Mag, 1977, 35: 549 – 565.

[24] Crawford R C. Deformation of an ordered Fe-35.5 at % Al alloy [J]. Phll Mag, 1976, 33: 529– 555.

(Edited by YANG Bing)